Phys Chem Minerals (2003) 30: 401–408
DOI 10.1007/s00269-003-0336-0

ORIGINAL PAPER

F. Martignago · A. Dal Negro · S. Carbonin

How Cr^{3+} and Fe^{3+} affect Mg–Al order–disorder transformation at high temperature in natural spinels

Received: 3 February 2003 / Accepted: 22 May 2003

Abstract Three natural $Mg(Al_{2-y}Cr_y)O_4$ spinels (y ~0.07–0.16), highly ordered in terms of Mg–Al, and one $Mg(Al_{2-y}Fe^{3+}_y)O_4$ spinel (y~0.08), highly ordered also in terms of Fe^{3+}, were studied by means of X-ray single-crystal diffraction. All samples were heated in situ from 25 to 1000 °C in order to follow both thermal expansion and evolution of the structural state of spinel with temperature. Thermal expansion was monitored by means of the variation of cell edge a with temperature, and found to be well represented throughout the temperature range by a regression line $a = a_0\ (1 + \alpha\Delta T)$, slightly different at lower and higher temperatures. Thermal expansion coefficient α_1, referring to the lower temperature range (i.e. during pure thermal expansion), was slightly lower than α_2, calculated only over the highest temperatures. The trend showed different slopes for individual crystals.

Structural evolution with temperature was studied by means of the variation of oxygen positional parameter u, which is strongly influenced by intersite cation exchange and thus closely correlated with inversion parameter x. In particular, in the three Cr samples, in which Cr resides only in the octahedral site, u parameter variations and hence the order–disorder process, started at about 700 °C. Instead, in the Fe^{3+} sample, this process was triggered at lower temperatures, starting at 550 °C with Fe^{3+}–Mg exchange followed at higher temperatures by that of Mg–Al. Cr contents in the Cr samples affected the occupancy of Al in the tetrahedral site at the highest temperatures.

In both Mg–Al–Cr and Mg–Al–Fe^{3+} compositions, if Cr~Fe^{3+}, parameter u reached the same value only when the Mg–Al exchange was dominant, i.e. at the highest temperatures, but not before.

Cation distribution at each temperature was obtained by the bond-length model, applying thermal expansion to pure bond lengths. This method is applied here to complex compositions for the first time.

Keywords In situ heating · Cr^{3+} spinel · Fe^{3+} spinel · X-ray diffraction · Order–disorder

F. Martignago (✉) · A. Dal Negro · S. Carbonin
Dipartimento di Mineralogia e Petrologia,
Università di Padova, Corso Garibaldi 37, 35137 Padova, Italy
e-mail: Fedora@dmp.unipt.it
Tel.: + +39 049 8272032
Fax + +39 049 8272010

Introduction

The temperature dependence of the cation distribution between T and M sites in spinels has been extensively studied by means of several analytical techniques and heating methods (in situ and quench) such as: NMR (Wood et al. 1986; Millard et al. 1992; Maekawa et al. 1997), ESR (Schmocker and Waldner 1976), powder neutron diffraction (Peterson et al. 1991; Harrison et al. 1999; Redfern et al. 1999), magnetic susceptibility (Harrison and Putnis 1999), Mössbauer spectroscopy (O'Neill et al. 1992; Larsson 1995; Andreozzi et al. 2001) and powder and single-crystal X-ray diffraction (Yamanaka and Takeuchi 1983; O'Neill and Dollase 1994; O'Neill et al. 1992; Della Giusta et al. 1996; Andreozzi et al. 2000; Carbonin et al. 2002). However, most of these studies were performed on synthetic samples (end members or binary joins) obtained from material quenched from high annealing temperatures, and thus characterized by high structural disorder. Comparatively, only a few of the above works regard natural spinels, which show a much lower inversion degree at room temperature, due to ordering during very slow continuous cooling on a geological time scale. Moreover, studies based on in situ heating are scarce, although such experiments are really the best way to obtain information on high-temperature intracrystalline cation distribution, not influenced by effects due to quenching processes. For these reasons, highly ordered natural spinels belonging to the series spinel–magnesiochromite and spinel–magnesioferrite, characterized by Cr^{3+} or Fe^{3+} cations substituting for

Al^{3+}, were studied by means of single-crystal X-ray diffraction and in situ heating. The aim of this work was to understand how Cr^{3+} and Fe^{3+} cations influence the Mg–Al order–disorder reaction with temperature.

Selected specimens were three pink Mg–Al–Cr spinels from the Olkhon metamorphic complex, Lake Baikal, Russia (Makrygina and Petrova 1998; Lavina et al. 2003), characterized by increasing chromium contents from 0.07 (L–Cr) to 0.12 (M–Cr) and 0.16 (H–Cr) atoms per four oxygens. The fourth sample (L–Fe^{3+}) is a green ferrian variety (obsolete mineral name: chlorospinel) from the Shishimsk Mountains, Urals, Russia, occurring in a chlorite schist with magnetite (Bothwell and Hey 1958).

It is well known in the literature that the Cr^{3+} cation is completely ordered in the M site (Navrotsky and Kleppa 1967; Burns 1975; O'Neill and Dollase 1994), as well as that the Fe^{3+} cation often shows an essentially ordered distribution in the octahedral site in natural samples (Osborne et al. 1981; Carbonin et al. 1996; Della Giusta et al. 1996; Lucchesi and Della Giusta 1997).

On the basis of similar contents of Fe^{3+} (0.08 atoms per four oxygens) and Cr^{3+} (0.07), and the ordering of both cations in the M site, L–Fe^{3+} and L–Cr samples were compared.

Oxygen positional parameter u was chosen to monitor the evolution of the spinel structural state, as it may be measured routinely with extreme accuracy and precision. Cation distribution at each temperature was obtained by the bond-length model, applying thermal expansion to pure bond lengths. This method is applied here to complex compositions for the first time.

Experimental

Data collection

X-ray single-crystal data were collected up to $2\theta = 75°$ (Mokα radiation monochromatized by a flat graphite crystal) using a Siemens Aed II 4-circle diffractometer. For each crystal, the same set of 87 independent reflections were measured using the ω-2θ scan mode, with profile recording for each reflection, and then used for all heating runs. Intensity data were collected from room temperature to 1000 °C in a controlled atmosphere (Ar) using a microfurnace installed on the diffractometer (Molin et al. 2001; Carbonin et al. 2002). The time for most data collections was about 2 h, including the time required for orientation matrix and cell parameter measurement (50 min). At 700 °C, on the basis of the kinetic data from the literature (Andreozzi and Princivalle 2002), the crystal was maintained at the same temperature for about 15 h before data collection, in order to approach equilibrium as closely as possible. However, it is our opinion, that until 650 °C the equilibrium distribution was obviously not achieved considering the time used for the experiments. Moreover, in order to define at which temperature intracrystalline reactions begin, several back-and-forth runs were carried out, continuously monitoring at each temperature oxygen coordinate u, which is order–disorder transformation-dependent at a given temperature.

For all heating runs, intensities were corrected for spherical absorption by taking into account the mean radius of the crystal.

Unit-cell parameters were determined at each temperature by centering 24 reflections in the range $25° < \theta < 34°$. Each reflection was centered at both positive and negative values of 2θ and ω angles using the double-step scan routine. The mean of the ω centres was taken as the true value.

Refinements

Structural refinements were carried out in the $Fd\bar{3}m$ space group (with origin at $\bar{3}$ m) with the Shelxl-97 program (Sheldrick 1997) without chemical constraints. No violations of this symmetry were detected. Refined parameters were: scale factor, secondary extinction coefficient, oxygen positional parameter u, anisotropic displacement parameters U(O), U(M) and U(T). For L–Cr^{3+} and L–Fe^{3+} samples, one scattering curve, Mg^{2+} and $Al^{1.5+}$, was assigned to T and M sites, respectively, not constrained to full site occupancy because of the Mg–Al inversion. For M–Cr^{3+} and H–Cr^{3+} samples, Mg^{1+} and two scattering curves, $Al^{1.5+}$ and $Cr^{1.5+}$, were assigned to T and M sites, respectively.

In spinels, the mean atomic number (m.a.n.) determined by least-squares refinement of site occupancies is quite sensitive to the ionization level of oxygen (Della Giusta et al. 1986) so, for the O-scattering curve, an ionization level between $O^{1.5-}$ and O^{2-} was chosen to obtain the best values for all conventional agreement factors.

Structural refinement results are listed in Tables 1 and 2.

Sample characterization

After data collection, chemical analyses were performed on the polished surface of the same single crystal used for X-ray study, using the Cameca/Camebax Microbeam electron microprobe at the Istituto di Geoscienze e Georisorse, CNR Padova. Analyses were performed at 15 kV and 15 nA sample current using the wavelength-dispersive method (WDS). X-ray counts were converted into oxide weight percentages using the PAP correction program supplied by CAMECA. Synthetic spinel ($MgAl_2O_4$) and synthetic oxide standards were used. The results of the microprobe analyses are reported in Table 3.

Inversion parameter x (Al in T) at room temperature was calculated according to the bond-length method, following Carbonin et al. (1996) and using ionic radii at room temperature from Lavina et al. (2002). This method determines cation distribution by using a soft chemical constraint. At the temperature at which cation exchange occurs, the x variation was determined with the same method as before, by applying thermal expansion coefficient α_1 (see next section) to pure bond lengths (Carbonin et al. 2002).

Results and discussion

The variation of cell edge a with temperature is clearly shown by two regression lines $a = a_0 (1 + \alpha\Delta T)$, slightly different at lower and higher temperatures and with different slopes for individual crystals. Thermal expansion coefficient α_1, referring to the lower temperature range (i.e. during pure thermal expansion, preceding the variation in parameter u) is slightly lower than α_2, calculated only over the highest temperatures (Fig. 1). The best-fit values of the coefficients of these equations are listed in Table 4.

Oxygen positional parameter u is greatly influenced by intersite cation exchange, which is temperature-dependent, and thus closely correlated with inversion parameter x; for this reason u is considered as a good

Table 1 Structural refinement results in samples L–Cr, M–Cr and H–Cr (estimated standard deviation *in brackets*). Number of non-equivalent reflections: 87 for all runs

T (°C)	a (Å)	u	x[a]	U_{eq}(O) (Å^2)	U_{eq}(M) (Å^2)	U_{eq}(T) (Å^2)	e^-(M)	e^-(T)	e^-tot	MO (Å)	TO (Å)	R_{all}[b] %	wR_2[b] %
L–Cr													
1st run													
25	8.0914(11)	0.26344(8)	0.121	0.0046(2)	0.0042(2)	0.0050(3)	13.51(5)	12.29(7)	39.30(12)	1.920(1)	1.940(1)	2.01	2.96
200	8.1018(11)	0.26355(8)	0.113	0.0061(3)	0.0058(2)	0.0070(3)	13.58(6)	12.36(8)	39.51(14)	1.922(1)	1.944(1)	2.47	2.93
400	8.1169(10)	0.26337(9)	0.126	0.0082(3)	0.0083(2)	0.0099(4)	13.67(7)	12.36(8)	39.71(16)	1.927(1)	1.945(1)	2.70	2.85
450	8.1207(10)	0.26348(8)	0.118	0.0091(3)	0.0088(2)	0.0109(3)	13.62(5)	12.40(7)	39.65(13)	1.927(1)	1.948(1)	2.57	2.59
400	8.1168(10)	0.26327(8)	0.134	0.0083(3)	0.0083(2)	0.0096(3)	13.62(5)	12.33(7)	39.57(13)	1.927(1)	1.944(1)	2.72	2.97
25	8.0917(10)	0.26346(7)	0.119	0.0043(2)	0.0043(2)	0.0052(3)	13.62(5)	12.38(6)	39.61(12)	1.920(1)	1.941(1)	2.01	2.38
2nd run													
500	8.1256(8)	0.26329(10)	0.132	0.0102(4)	0.0094(2)	0.0113(4)	13.54(7)	12.26(9)	39.34(16)	1.929(1)	1.946(1)	3.42	3.04
450	8.1217(8)	0.26337(9)	0.126	0.0093(3)	0.0090(2)	0.0105(4)	13.57(6)	12.24(8)	39.39(15)	1.928(1)	1.946(1)	2.71	2.70
3rd run													
550	8.1298(9)	0.26346(8)	0.119	0.0103(3)	0.0101(2)	0.0121(3)	13.59(6)	12.31(7)	39.48(13)	1.929(1)	1.950(1)	3.16	2.55
600	8.1335(10)	0.26342(9)	0.122	0.0111(3)	0.0106(2)	0.0135(4)	13.68(6)	12.46(7)	39.82(14)	1.930(1)	1.950(1)	3.24	2.78
650	8.1381(7)	0.26333(9)	0.129	0.0124(3)	0.0113(2)	0.0134(4)	13.52(5)	12.25(8)	39.29(14)	1.932(1)	1.950(1)	2.94	3.16
700	8.1423(10)	0.26210(11)	0.223	0.0164(4)	0.0128(3)	0.0147(4)	13.43(6)	12.38(8)	39.23(15)	1.942(1)	1.933(2)	3.34	2.94
800	8.1503(11)	0.26165(11)	0.257	0.0183(4)	0.0147(3)	0.0155(4)	13.47(7)	12.33(8)	39.26(15)	1.947(1)	1.929(2)	4.28	3.08
900	8.1577(11)	0.26132(12)	0.283	0.0190(4)	0.0159(3)	0.0168(5)	13.65(6)	12.49(9)	39.79(16)	1.951(1)	1.926(2)	4.16	3.59
1000	8.1667(14)	0.26118(15)	0.293	0.0207(5)	0.0174(4)	0.0184(6)	13.67(7)	12.57(12)	39.92(19)	1.955(1)	1.926(2)	5.08	4.58
M–Cr													
1st run													
28	8.1019(10)	0.26346(10)	0.114	0.0057(5)	0.0055(3)	0.0051(4)	13.69(58)	12.13(10)	39.51(1.16)	1.923(1)	1.943(1)	4.19	3.02
200	8.1116(10)	0.26343(11)	0.117	0.0076(5)	0.0068(3)	0.0073(4)	13.62(62)	12.13(11)	39.37(1.24)	1.925(1)	1.945(2)	4.21	3.15
400	8.1263(10)	0.26344(10)	0.116	0.0097(5)	0.0088(2)	0.0098(4)	13.72(54)	12.23(9)	39.66(1.08)	1.929(1)	1.949(1)	3.74	2.58
450	8.1305(7)	0.26336(14)	0.122	0.0101(6)	0.0097(3)	0.0111(6)	13.81(78)	12.36(13)	39.97(1.56)	1.930(1)	1.948(2)	4.54	3.75
400	8.1265(9)	0.26330(10)	0.127	0.0101(5)	0.0089(3)	0.0099(4)	13.62(57)	12.14(9)	39.38(1.15)	1.930(1)	1.947(1)	3.71	2.70
28	8.1018(10)	0.26348(10)	0.113	0.0052(4)	0.0055(2)	0.0054(4)	13.83(56)	12.31(10)	39.98(1.12)	1.922(1)	1.943(1)	3.87	3.00
2nd run													
500	8.1338(9)	0.26343(10)	0.117	0.0108(5)	0.0100(3)	0.0113(4)	13.61(58)	12.15(9)	39.36(1.17)	1.930(1)	1.950(1)	3.97	2.82
450	8.1302(8)	0.26334(12)	0.124	0.0108(6)	0.0094(3)	0.0104(5)	13.71(68)	12.16(11)	39.58(1.36)	1.930(1)	1.948(2)	4.43	3.26
3rd run													
550	8.1379(9)	0.26339(12)	0.120	0.0114(6)	0.0103(3)	0.0121(5)	13.81(70)	12.33(11)	39.94(1.40)	1.932(1)	1.951(2)	4.70	3.43
600	8.1419(11)	0.26331(14)	0.126	0.0135(6)	0.0112(3)	0.0126(6)	13.58(78)	12.05(12)	39.21(1.57)	1.933(1)	1.950(2)	4.51	4.13
650	8.1461(9)	0.26308(12)	0.143	0.0145(6)	0.0117(3)	0.0135(5)	13.43(71)	12.07(11)	38.94(1.43)	1.936(1)	1.948(2)	5.15	3.43
700	8.1502(9)	0.26231(15)	0.202	0.0179(7)	0.0131(4)	0.0135(6)	13.40(85)	11.92(13)	38.72(1.71)	1.942(1)	1.938(2)	5.80	4.57
800	8.1577(8)	0.26187(16)	0.236	0.0178(7)	0.0146(4)	0.0144(7)	13.68(94)	12.21(13)	39.58(1.89)	1.947(1)	1.934(2)	6.03	4.64
900	8.1658(12)	0.26151(13)	0.263	0.0209(6)	0.0158(4)	0.0167(6)	13.42(77)	12.25(10)	39.09(1.53)	1.952(1)	1.931(2)	5.65	3.49
1000	8.1733(4)	0.26144(12)	0.267	0.0212(7)	0.0170(4)	0.0182(6)	13.71(78)	12.61(11)	40.03(1.57)	1.954(1)	1.932(2)	5.81	3.11
H–Cr													
1st run													
25	8.1080(12)	0.26338(10)	0.114	0.0049(4)	0.0048(2)	0.0046(4)	14.07(59)	12.27(10)	40.40(1.18)	1.925(1)	1.943(1)	2.98	3.41
200	8.1180(11)	0.26331(12)	0.120	0.0065(4)	0.0063(3)	0.0068(4)	14.09(69)	12.35(12)	40.53(1.38)	1.927(1)	1.945(2)	2.73	4.42
400	8.1316(10)	0.26348(11)	0.107	0.0088(5)	0.0082(3)	0.0098(4)	14.12(60)	12.45(10)	40.68(1.21)	1.929(1)	1.950(2)	4.05	3.27
450	8.1354(11)	0.26343(11)	0.111	0.0095(5)	0.0089(3)	0.0109(5)	13.97(62)	12.40(11)	40.34(1.25)	1.931(1)	1.951(2)	4.32	3.34

Table 1 (Contd.)

T (°C)	a (Å)	u	x[a]	U_{eq}(O) (Å^2)	U_{eq}(M) (Å^2)	U_{eq}(T) (Å^2)	e$^-$(M)	e$^-$(T)	e$^-$tot	MO (Å)	TO (Å)	R_{all}[b] %	wR_2[b] %
400	8.1315(14)	0.26348(11)	0.107	0.0085(5)	0.0079(3)	0.0099(4)	14.01(61)	12.42(10)	40.44(1.22)	1.929(1)	1.950(2)	3.85	3.39
25	8.1085(8)	0.26327(10)	0.123	0.0056(4)	0.0045(2)	0.0050(4)	13.86(56)	12.18(10)	39.90(1.12)	1.925(1)	1.942(1)	2.99	3.36
2nd run													
500	8.1400(14)	0.26346(12)	0.109	0.0105(5)	0.0093(3)	0.0114(5)	13.86(67)	12.30(11)	40.02(1.34)	1.932(1)	1.952(2)	3.94	3.78
450	8.1358(13)	0.26358(10)	0.099	0.0098(5)	0.0088(2)	0.0105(4)	13.92(55)	12.31(9)	40.14(1.11)	1.930(1)	1.953(1)	3.93	2.84
3rd run													
550	8.1445(6)	0.26355(10)	0.101	0.0094(5)	0.0101(3)	0.0124(4)	14.42(59)	12.69(10)	41.52(1.19)	1.932(1)	1.954(1)	3.52	2.94
600	8.1482(8)	0.26342(11)	0.111	0.0123(5)	0.0107(3)	0.0134(5)	13.95(62)	12.36(10)	40.26(1.24)	1.934(1)	1.953(2)	4.22	3.11
650	8.1525(6)	0.26318(12)	0.129	0.0130(5)	0.0116(3)	0.0142(5)	13.99(67)	12.40(11)	40.39(1.34)	1.937(1)	1.951(2)	4.57	3.44
700	8.1569(7)	0.26242(12)	0.187	0.0149(5)	0.0127(3)	0.0138(5)	14.11(67)	12.43(11)	40.64(1.35)	1.943(1)	1.941(2)	4.44	3.37
800	8.1655(5)	0.26221(13)	0.204	0.0166(7)	0.0140(3)	0.0162(5)	14.09(74)	12.65(12)	40.83(1.49)	1.947(1)	1.941(2)	5.98	3.27
900	8.1726(11)	0.26197(11)	0.222	0.0187(6)	0.0154(3)	0.0170(5)	14.02(63)	12.57(10)	40.60(1.26)	1.950(1)	1.939(2)	5.19	2.62
1000	8.1791(9)	0.26171(13)	0.242	0.0205(7)	0.0168(4)	0.0187(6)	14.03(76)	12.62(12)	40.67(1.53)	1.954(1)	1.937(2)	6.36	3.27

[a] x inversion degree
[b] R_{all} and wR2 agreement factors according to SHELXL97 program package

Table 2 Structural refinement results in sample L–Fe^{3+} (estimated standard deviation *in brackets*). Number of non-equivalent reflections: 87 for all runs

T (°C)	a (Å)	u	x[a]	U_{eq} (O) (Å^2)	U_{eq} (M) (Å^2)	U_{eq} (T) (Å^2)	e$^-$(M)	e$^-$(T)	e$^-$tot	MO (Å)	TO (Å)	R_{all}[b] (%)	wR_2[b] (%)
L–Fe^{3+}													
1st run													
25	8.0989(10)	0.26326(7)	0.141	0.0047(2)	0.0043(2)	0.0048(2)	13.62(5)	12.67(6)	39.90(11)	1.923(1)	1.926(1)	1.94	2.51
200	8.1092(6)	0.26329(8)	0.139	0.0062(3)	0.0059(2)	0.0070(3)	13.63(5)	12.67(7)	39.93(12)	1.923(1)	1.926(1)	2.30	3.13
400	8.1239(6)	0.26333(8)	0.136	0.0088(3)	0.0081(2)	0.0098(3)	13.65(5)	12.76(7)	40.06(12)	1.929(1)	1.946(1)	2.30	2.73
450	8.1281(7)	0.26323(9)	0.142	0.0099(3)	0.0090(2)	0.0103(3)	13.53(5)	12.57 (8)	39.64(13)	1.930(1)	1.946(1)	2.42	3.212
400	8.1243(6)	0.26336(7)	0.132	0.0096(3)	0.0081(2)	0.0094(3)	13.42(5)	12.42(7)	39.27(11)	1.939(1)	1.947(1)	2.38	2.65
25	8.0987(6)	0.26325(8)	0.138	0.0049(2)	0.0045(2)	0.0044(3)	13.55(5)	12.48(7)	39.58(13)	1.923(1)	1.939(1)	2.30	3.05
2nd run													
500	8.1318(5)	0.26331(8)	0.138	0.0104(3)	0.0096(2)	0.0110(3)	13.51(5)	12.58(7)	39.61(12)	1.931(1)	1.948(1)	2.13	2.70
450	8.1280(6)	0.26337(8)	0.132	0.0100(3)	0.0090(2)	0.0106(3)	13.57(5)	12.63(7)	39.78(12)	1.929(1)	1.948(1)	2.17	3.02
3rd run													
550	8.1359(6)	0.26327(10)	0.146	0.0112(4)	0.0103(3)	0.0118(4)	13.62(7)	12.80(9)	40.05(17)	1.932(1)	1.948(1)	3.10	3.05
600	8.1403(7)	0.26292(8)	0.172	0.0134(3)	0.0112(2)	0.0121(3)	13.38(5)	12.67(6)	39.43(12)	1.936(1)	1.945(1)	2.86	2.53
650	8.1440(7)	0.26250(9)	0.210	0.0153(4)	0.0118(2)	0.0128(4)	13.27(5)	12.78(7)	39.32(13)	1.940(1)	1.940(1)	3.28	2.98
700	8.1469(7)	0.26190(10)	0.258	0.0167(4)	0.0127(3)	0.0139(4)	13.21(6)	12.91(7)	39.34(14)	1.945(1)	1.932(1)	3.95	3.08
800	8.1547(8)	0.26159(10)	0.278	0.0186(4)	0.0143(2)	0.0148(4)	13.17(5)	12.88(7)	39.22(12)	1.949(1)	1.929(1)	3.46	3.26
900	8.1627(9)	0.26133(9)	0.297	0.0199(4)	0.0160(3)	0.0163(4)	13.32(5)	13.01(7)	39.64(13)	1.953(1)	1.927(1)	3.69	2.79
1000	8.1701(10)	0.26116(12)	0.309	0.0219(5)	0.0171(3)	0.0178(4)	13.33(6)	13.04(9)	39.70(15)	1.956(1)	1.927(2)	4.26	3.63

[a] x inversion degree (Al + Fe^{3+})
[b] R_{all} and wR2 agreement factors according to SHELXL97 program package

Table 3 Chemical composition by electron microprobe. Average of 20 to 33 analyses. (estimated standard deviation *in brackets*)

Sample	L–Cr	M–Cr	H–Cr	L–Fe^{3+}
MgO	28.04 (28)	27.85 (37)	27.71 (36)	27.93 (21)
Al_2O_3	68.14 (56)	65.89 (64)	64.59 (95)	68.06 (42)
Cr_2O_3	3.51 (14)	6.49 (23)	8.50 (75)	–
MnO	0.03 (3)	0.09 (4)	0.09 (3)	0.07 (5)
ZnO	0.10 (7)	0.41 (7)	0.37 (7)	0.20 (8)
FeO	–	–	–	3.93 (12)
Σ	99.82	100.73	101.26	100.19
Cations on basis of four oxygens				
Mg	1.003 (5)	0.999 (9)	0.995 (9)	0.997 (6)
Al	1.928 (6)	1.868 (13)	1.834 (19)	1.920 (6)
Cr^{3+}	0.066 (3)	0.123 (4)	0.162 (14)	–
Mn	0.001 (1)	0.002 (1)	0.002 (1)	0.001 (1)
Zn	0.002 (1)	0.007 (1)	0.007 (1)	0.003 (1)
Fe^{3+}	–	–	–	0.079 (3)
Σ	3.000	2.999	3.000	3.000

indicator for monitoring the structural state evolution of the spinel as a function of temperature.

In order to identify the temperature at which the cation exchange begins (transition zone), the three crystals with different Cr^{3+} contents and the L–Fe^{3+} sample were subjected to several back-and-forth runs at lower temperatures (from room temperature up to 500 °C). During these heating runs, the oxygen coordinate remained constant and thermal expansion was completely reversible, because no changes in the degree of order were evident.

Figure 2 shows variations in oxygen positional parameter *u* as a function of temperature for the three Cr^{3+} samples. The *u* value clearly remains constant for the three samples up to 600 °C, independently of Cr^{3+} contents. From this temperature onwards, the disordering pathways show two different slopes, between

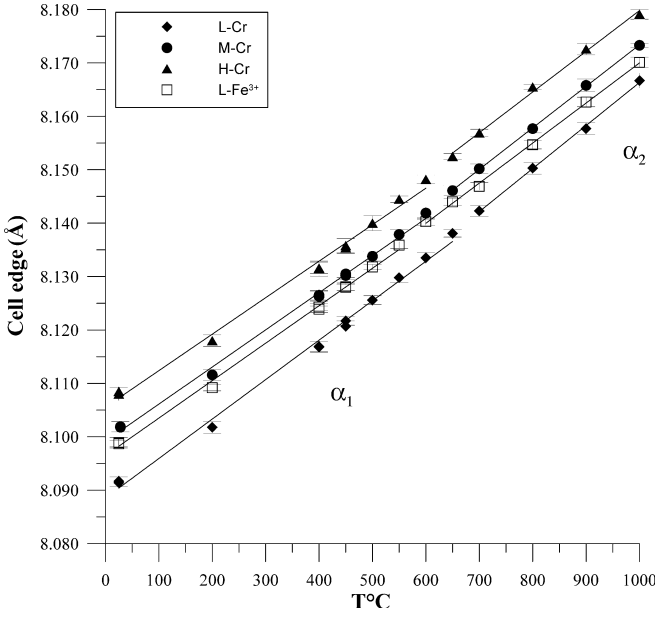

Fig. 1 Cell edge vs. temperature. In each sample, two regression lines before and after transition zone are calculated with slightly different α_1 and α_2 thermal expansion coefficients

600 and 700 °C and 700 and 1000 °C, in all samples. From 600 to 650 °C, the samples slowly begin to disorder, M–Cr and H–Cr slightly more than L–Cr. Instead, from 650 to 700 °C, *u* suddenly drop in all samples, and at 700°C sample L–Cr reverses the above trend, reaching the lowest *u* value. Parameter *u* then decreases continuously reaching, along different pathways, quite different values at 1000 °C: 0.2612(1), 0.2615(1) and 0.2617(1), with a degree of inversion *x* of 0.29, 0.27 and 0.24 in L–Cr, M–Cr and H–Cr respectively. The degree of disorder reached at the highest temperature is inversely correlated with Cr^{3+} contents, which therefore limit Mg–Al exchange, due to the preference of Cr^{3+} for the octahedral site.

On the basis of different kinds of non-aluminium trivalent cations (Cr^{3+} vs Fe^{3+}) but with similar contents ($Cr^{3+} = 0.07$; $Fe^{3+} = 0.08$ atoms per four oxygens), it was possible to compare L–Cr with L–Fe^{3+}. Both samples are highly ordered in terms of Mg–Al and, in addition, L–Fe^{3+} shows Fe^{3+} cation mainly ordered in M site (Lucchesi and Della Giusta 1997).

Figure 3 shows variations in oxygen positional parameter *u*, as a function of temperature. It is evident how the transition zone is different between the two samples: in L–Fe^{3+} the exchange reaction starts between 550 and 600 °C, and in L–Cr^{3+} at 650 °C. From these temperatures, both the *u* values show abrupt changes up to 700 °C, whereas from 800 to 1000 °C they show gentle changes, following the same disordering pathways and finally reaching the same values [0.2612(1)]. The same trend is shown by inversion parameter *x*, with the greatest differences between the two samples in the range 550–700 °C (e.g. at 650 °C $x = 0.210$ in L–Fe^{3+} and 0.129 in L–Cr) and only slight between 800 and 1000 °C (e.g. at 1000 °C $x = 0.309$ in L–Fe^{3+} and 0.293 in L–Cr). This difference in *x* between 550 and 700 °C is due to the different electron density in M and T sites.

Figure 4 shows qualitatively how the distribution of electrons between M and T sites ($(2eM\text{-}eT)/e_{Tot}$) changes in L–Fe^{3+} from 550 to 700 °C and remains constant from 700 to 1000 °C; instead, in L–Cr there are no sig-

Table 4 Best-fit values of thermal expansion coefficient in linear regression $a = a_0(1+\alpha\Delta T)$ α_1: lower temperature range; α_2: highest temperatures

Sample	T range (°C)	a_0 (Å)	$\alpha_1 \times 10^{-6}$ (°C^{-1})	$\alpha_2 \times 10^{-6}$ (°C^{-1})	R^2
L–Cr	25–650	8.0906 (7)	9.0 (2)		0.995
	700–1000	8.0880 (2)		9.9 (3)	0.998
M–Cr	25–600	8.1011 (5)	8.6 (2)		0.997
	650–1000	8.0977 (3)		9.57 (5)	1.000
H–Cr	25–600	8.1074 (8)	8.5 (2)		0.994
	650–1000	8.1050 (3)		9.6 (4)	0.994
L–Fe^{3+}	25–550	8.0980 (5)	8.7 (2)		0.997
	600–1000	8.0970 (1)		9.2 (2)	0.999

nificant changes at any temperature. Actually, according to detectable or undetectable differences in electrons in the two samples, Fe^{3+} cations migrate from M to T site; alternatively, the exchange mainly involves Mg and Al. Table 5 shows how, in L–Fe^{3+} in the T site, Mg starts exchanging with Fe^{3+} between 500 and 550 °C, while Al remains constant up to 550 °C; between 550 and 600 °C Mg exchanges only with Al, this exchange also remaining dominant from 600 up to 700 °C with respect to that of Fe^{3+}–Mg. From 700 to 1000 °C, the only detectable exchange is Mg–Al. Table 1 shows that in L–Cr, Al remains constant up to 650 °C in the T site and then significantly increases from 700 to 1000 °C.

Figure 5 shows Fe^{3+} mainly ordered in the M site (80%) from room temperature up to 500 °C, but from 550 to 700 °C Fe^{3+} it disorders in the T site up to ~ 50%, and then, from 700 to 1000 °C, it reorders slightly in the M site. The same behaviour is confirmed by recent studies performed on synthetic spinel–magnesioferrite series by Mössbauer spectroscopy (Andreozzi et al. 2001), showing Fe^{3+} partitioning as a function of magnesioferrite components and temperature. Unfortunately, these synthetic samples have a final equilibrium temperature estimated to be around 800 °C, and therefore Fe^{3+} behaviour is comparable with that found in L–Fe^{3+} only at the highest temperatures (800–1000 °C), with a slight preference of the Fe^{3+} cation for the M site.

The behaviour of Fe^{3+}, in spite of its low amount in the sample, supports the idea that at the lowest temperature, our data are consistent with a two-stage kinetic process in which relatively rapid exchange of Fe^{3+} with Mg between tetrahedral and octahedral sites is followed by slower exchange of Mg with Al, as observed by Harrison et al. (1999). For this purpose, in situ heating of the disordering kinetics at different isotherms can highlight such a two-stage process, and study is in progress on this natural sample in the range 500–700 °C. It will be interesting to compare results with those of the equivalent Cr sample.

Summary

In the three Cr samples, oxygen positional parameter u and inversion parameter x values as a function of tem-

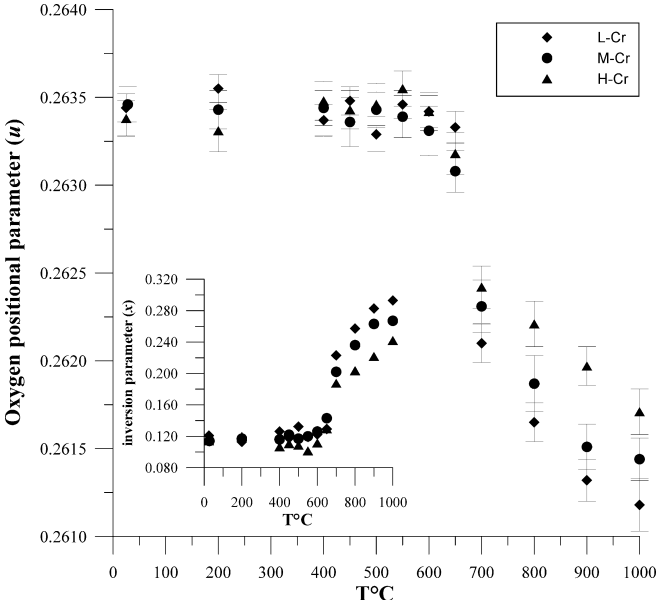

Fig. 2 Oxygen positional parameter u as a function of temperature in samples L–Cr, M–Cr and H–Cr. *Inset*: Inversion parameter x vs. temperature

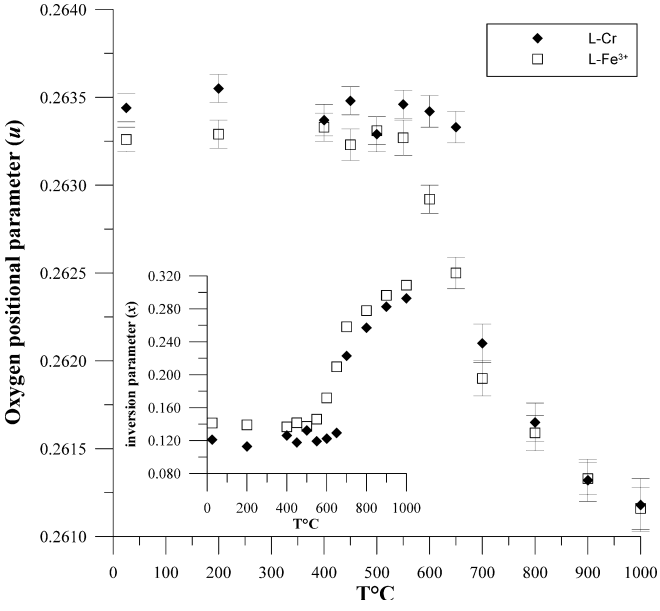

Fig. 3 Oxygen positional parameter u as a function of temperature in samples L–Fe^{3+} and L–Cr. *Inset*: Inversion parameter x vs. temperature

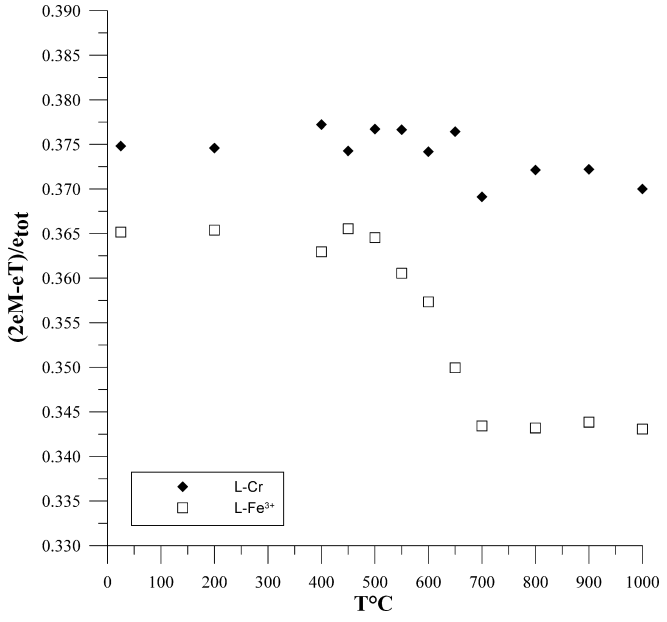

Fig. 4 Distribution of electrons between M and T sites obtained from structural refinements in samples L–Fe^{3+} and L–Cr, as a function of temperature, for forward runs only

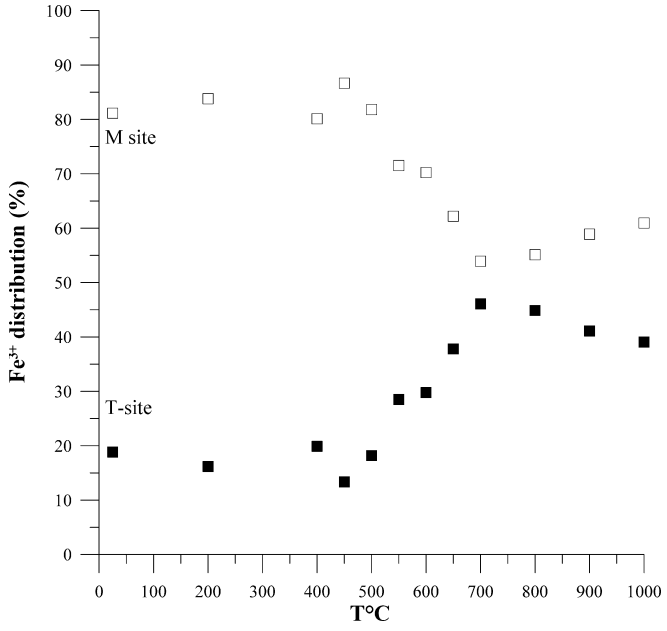

Fig. 5 Ferric iron distribution (%) as a function of temperature in sample L–Fe^{3+}, obtained by cation partitioning (Table 5). *Solid and open squares* Relative proportions of Fe^{3+} in T and M sites respectively, for forward runs only

perature are related to Cr content, which therefore affects Mg–Al exchange. In sample L–Cr, *u* reaches the lowest and *x* the highest values, opposite to what occurs in sample H–Cr.

In sample L–Fe^{3+}, *u* reaches the same value as in sample L–Cr at the highest temperatures, showing the same disordering pathways from 800 to 1000 °C, and therefore similar values of *x*, whereas those between 550 and 700 °C are significantly different. In this region, inversion parameter *x* (Al^{3+} + Fe^{3+}) in L–Fe^{3+} is due to rapid Fe^{3+}–Mg exchange between M and T sites, and at 800–1000 °C it is due to prevalent Mg–Al exchange, suggesting a two-stage kinetic process. Therefore Cr and Fe^{3+}, when substituting for Al in equal amounts, affect high-temperature behaviour in the spinel in different ways. Whereas Cr contents limit Mg–Al exchange, not starting before 700 °C, Fe^{3+} triggers trivalent–divalent cation exchange starting from 550 °C.

The model adopted here to determine cation distributions from bond lengths determined in situ seems to be reliable also for complex compositions.

Table 5 Al, Fe^{3+} and Mg distribution between T and M sites as a function of temperature in sample L–Fe^{3+}

T (°C)	T site			M site		
	Al	Fe^{3+}	Mg	Al	Fe^{3+}	Mg
L–Fe^{3+}						
1st run						
25	0.126	0.015	0.847	1788	0.067	0.143
200	0.126	0.013	0.850	1.791	0.068	0.138
400	0.120	0.016	0.852	1.795	0.066	0.137
450	0.131	0.011	0.849	1.786	0.069	0.143
400	0.120	0.012	0.860	1.799	0.067	0.133
25	0.131	0.007	0.852	1.786	0.073	0.139
2nd run						
500	0.123	0,015	0,853	1,795	0,065	0,138
450	0.118	0,014	0,857	1,798	0,067	0,133
3rd run						
550	0.123	0.023	0.844	1.794	0.057	0.147
600	0.148	0.024	0.819	1.769	0.056	0.174
650	0.180	0.030	0.781	1.735	0.050	0.214
700	0.221	0.037	0.733	1.693	0.043	0.263
800	0.242	0.036	0.714	1.672	0.044	0.282
900	0.263	0.034	0.695	1.649	0.048	0.300
1000	0.277	0.032	0.683	1.634	0.050	0.314

Acknowledgements This research was carried out with the financial support of an MIUR grant (A. Della Giusta Cofin 2001: Intracrystalline ordering–disordering process in rock-forming minerals). The Italian CNR financed the installation and maintenance of the microprobe laboratory at the University of Padova. Anna Koneva and Sergio Lucchesi generously supplied the samples for this study. Mr R. Carampin kindly assisted in microanalyses. The authors are grateful to Ms G. Walton for revising the English text. H. Skogby is thanked for his useful review.

References

Andreozzi GB, Princivalle F (2002) Kinetics of cation ordering in synthetic $MgAl_2O_4$ spinel. Am Mineral 87: 838–844

Andreozzi GB, Princivalle F, Skogby H, Della Giusta A (2000) Cation ordering and structural variations with temperature in $MgAl_2O_4$ spinel: an X-ray single-crystal study. Am Mineral 85: 1164–1171

Andreozzi GB, Hålenius U, Skogby H (2001) Spectroscopic active $^{IV}Fe^{3+}$–$^{VI}Fe^{3+}$ clusters in spinel-magnesioferrite solid solution crystals: a potential monitor for ordering in oxide spinels. Phys Chem Miner 28: 435–444

Bothwell DI, Hey MH (1958) The nature of chlorospinel. Mineral Mag 31: 885–887

Burns RG (1975) Crystal field effects in chromium and its partitioning in the mantle. Geochim Cosmochim Acta 39: 857–864

Carbonin S, Russo U, Della Giusta A (1996) Cation distribution in some natural spinels from X-ray diffraction and Mössbauer spectroscopy. Mineral Mag 60: 355–368

Carbonin S, Martignago F, Menegazzo G, Dal Negro A (2002) X-ray single-crystal study of spinels: in situ heating. Phys Chem Miner 29: 503–514

Della Giusta A, Princivalle F, Carbonin S (1986) Crystal chemistry of a suite of natural Cr-bearing spinels with $0.15 \leq Cr \leq 1.07$. Neues Jahrb Mineral Abh 155: 319–330

Della Giusta A, Carbonin S, Ottonello G (1996) Temperature-dependent disorder in a natural Mg–Al–Fe^{2+}–Fe^{3+}- spinel. Mineral Mag 60: 603–616

Harrison RJ, Putnis A (1999) Determination of the mechanism of cation ordering in magnesioferrite ($MgFe_2O_4$) from the time and temperature dependence of magnetic susceptibility. Phys Chem Miner 26:322–332

Harrison RJ, Dove MT, Knight KS, Putnis A (1999) In-situ neutron diffraction study of non-convergent cation ordering in the $(Fe_3O_4)_{1-x}$ $(MgAl_2O_4)_x$ spinel solid solution. Am Mineral 84: 555–563

Larsson L (1995) Temperature dependent cation distribution in a natural $Mg_{0.4}Fe_{0.6}Al_2O_4$ spinel. Neues Jahrb Miner Mh 4: 173–183

Lavina B, Salviulo G, Della Giusta A (2002) Cation distribution and structure modelling of spinel solid solutions. Phys Chem Miner 29: 10–18

Lavina B, Koneva A, Della Giusta A (2003) Cation distribution and cooling rates of Cr-substituted Mg-Al spinel from the Olkhon metamorphic complex, Russia. Eur J Mineral 15: 435–441

Lucchesi S, Della Giusta A (1997) Crystal chemistry of a highly disordered Mg-Al natural spinel. Mineral Petrol 59: 91–99

Maekawa H, Kato S, Kawamura K, Yokokawa T (1997) Cation mixing in natural $MgAl_2O_4$ spinel: a high temperature ^{27}Al NMR study. Am Mineral 82: 1125–1132

Makrygina VA, Petrova ZI (1998) The importance of geochemical data for geodynamic reconstruction: formation of the Olkhon metamorphic complex, Lake Baikal, Russia. Lithos 43: 135–150

Millard RL, Peterson RC, Hunter BK (1992) Temperature dependence of cation disorder in $MgAl_2O_4$ spinel, using ^{27}Al and ^{17}O magic-angle spinning NMR. Am Mineral 77: 44–52

Molin G, Martignago F, Dal Negro A (2001) A new radiative microfurnace for X-ray single-crystal diffractometry. Eur J Mineral 13: 557–563

Navrotsky A, Kleppa OJ (1967) The thermodynamics of cation distributions in simple spinels. J Inorg Nucl Chem 29:2701–2714

Osborne MD, Fleet ME, Bancroft GM (1981) Fe^{2+}–Fe^{3+} ordering in chromite and Cr-bearing spinels. Contrib Mineral Petrol 77: 251–255

O'Neill HStC, Annersten H, Virgo D (1992) The temperature dependence of the cation distribution in magnesioferrite ($MgFe_2O_4$) from powder XRD structural refinements and Mössbauer spectroscopy. Am Mineral 77: 725–740

O'Neill HStC, Dollase WA (1994) Crystal structures and cation distribution in simple spinels from powder XRD structural refinements: $MgCr_2O_4$, $ZnCr_2O_4$, Fe_3O_4 and the temperature dependence of the cation distribution in $ZnAl_2O_4$. Phys Chem Miner 20: 541–555

Peterson RC, Lager GA, Hitterman RL (1991) A time-of-flight neutron powder diffraction study of $MgAl_2O_4$ at temperatures up to 1273 K. Am Mineral 76: 1455–1458

Redfern SAT, Harrison RJ, O'Neill HStC, Wood DRR (1999) Thermodynamics and kinetics of cation ordering in $MgAl_2O_4$ spinel up to 1600 °C from in situ neutron diffraction. Am Mineral 84: 299–310

Schmocker U, Waldner F (1976) The inversion parameter with respect to the space group of $MgAl_2O_4$ spinels. J Phys C: Solid State Phys 9: L235–L237

Sheldrick G. M. (1997) SHELXL-97, a program for crystal structure refinement. University of Göttingen, Germany

Wood BJ, Kirkpatrick RJ, Montez B (1986) Order–disorder phenomena in $MgAl_2O_4$ spinel. Am Mineral 71: 999–1006

Yamanaka T, Takeuchi Y (1983) Order–disorder transition in $MgAl_2O_4$ spinel at high temperature up to 1700 °C. Z Kristallogr 165: 65–78